A refined finite element for first-order plate and shell analysis

Sung-Cheon Han[1a], Worsak Kanok-Nukulchai*[2] and Won-Hong Lee[3b]

[1]*Department of Civil and Railroad Engineering, Daewon University College, Jecheon 390-702, Korea*
[2]*School of Engineering and Technology, Asian Institute of Technology, Klongluang, Pathumthani, 12120, Thailand*
[3]*Department of Civil Engineering, Gyeongnam National University of Science and Technology, Jinju 660-758, Korea*

Abstract. This paper presents an improved 8-node shell element for the analysis of plates and shells. The finite element, based on a refined first-order shear deformation theory, is further improved by the combined use of assumed natural strain method. We analyze the influence of the shell element with the different patterns of sampling points for interpolating different components of strains. Using the assumed natural strain method with proper interpolation functions, the present shell element generates neither membrane nor shear locking behavior even when full integration is used in the formulation. Further, a refined first-order shear deformation theory, which results in parabolic through-thickness distribution of the transverse shear strains from the formulation based on the third-order shear deformation theory, is proposed. This formulation eliminates the need for shear correction factors in the first-order theory. Numerical examples demonstrate that the present element perform better in comparison with other shell elements.

Keywords: enhanced membrane and shear interpolation; locking behavior; full integration; refined first-order shear deformation theory; plates and shells

1. Introduction

As commonly accepted, two kinds of locking phenomena may occur in curved shear flexible bending element, namely shear and membrane lockings. While the shear locking may occur in both flat and curved shear-flexible bending element, the membrane locking occurs only in curved shell element. The classic 8-node isoparametric serendipity shell elements suffer shear locking when the thickness of the shell becomes too small. To avoid this phenomenon, some techniques of reduced/selective integrations have been proposed, Unfortunately, spurious zero-energy kinematic modes may occur and disturb the finite element response in a mesh.

To design an improved 8-node quadrilateral shell element, a standard procedure can be employed

---

*Corresponding author, Professor, E-mail: worsak@ait.ac.th
[a]Associate Professor
[b]Corresponding author, Professor, E-mail: whyee@gntech.ac.kr

to obtain the bending stiffness matrix. Special treatments are needed to evaluate the in-plane normal, the in-plane shear and the transverse shear strains. By a so-called "assumed strain method", the strain-displacement compatibility is fixed at discrete points leading to a surprisingly accurate results.

Bathe and Dvorkin (1986) proposed an eight-node shell element, named as MITC8, being free of membrane and shear locking. The strain tensor was expressed in terms of the covariant components and contravariant base vectors. The performance of this element was quite satisfactory and performed reasonably well in complex shell structures. Bucalem and Bathe (1993) have improved previous studies on the MITC8 shell elements (1986) and concluded that while it performed quite effectively, in certain cases the element exhibited very stiff behavior. Thus its improvement is warranted.

The 8-node shell element developed by Hinton and Huang (1986) passed relevant tests but its accuracy appeared to be inferior to the 9-node quadrilateral element. Lakshminarayana and Kailash (1989) used appropriately chosen interpolation functions based on Hinton and Huang's concept to derive a locking-free 8-node shell element.

Ma and Kanok-Nukulchai (1989) developed a 9-node assumed strain shell element based on the desirable displacement concept. Then Han *et al.* (2004, 2008) applied the same concept to develop a special shell element for laminated composite shells. In order to eliminate both the shear locking and membrane locking, the assumed strain method developed by Ma and Kanok-Nukulchai (1989) for the 9-node shell element was applied to the natural coordinate. Kim and Park (2002) and Kim *et al.* (2003) presented an 8-node shell finite element. In 8-node shell element, the persistence of locking problems was found to continue through numerical experiments on the standard test problem of MacNeal and Harder (1985).

So far a great number of 9-node shell elements show excellent performance (Bathe *et al.* 2003, Li *et al.* 2008, Wu *et al.* 2008) while only few 8-node shell elements perform reasonably. Although other works deal mostly with the 9-node Lagrangian quadrilateral element, it is not considered in this study as its internal node tends to cause problems in engineering practice.

The aim of this paper is to propose an improvement of the curved quadrilateral 8-node shell finite element, based on a refined higher-order shear deformation theory. In this new element, a new combination of sampling points for the assumed strain is proposed. The proposed shell element will also consider parabolic through-thickness distribution of the transverse shear stresses and strains based on simple corrections to the first-order theory proposed by Tanov and Tabiei (2000). The implementation was shown to be quite simple and straightforward (Han *et al.* 2008).

Finally, in order to validate the present shell element model, numerical examples are investigated and the results compared with other solutions in the literature.

2. Modified first-order shear deformation theory

The geometry of an 8-noded shell element with six degrees of freedom is shown in Fig. 1.

The higher-order shear deformation theory to be adopted in this study is based on the assumption that the originally straight normal to the mid surface can deform into a cubic-order function with respect to the thickness coordinate. Thus, we start with the third-order kinematic fields as follows

$$\mathbf{P}(\xi_i) = \overline{\mathbf{P}}(\xi_\beta) + \xi_3 \overline{\mathbf{V}}(\xi_j) + \xi_3^2 \mathbf{\Phi}(\xi_j) + \xi_3^3 \mathbf{\Psi}(\xi_j) \tag{1}$$
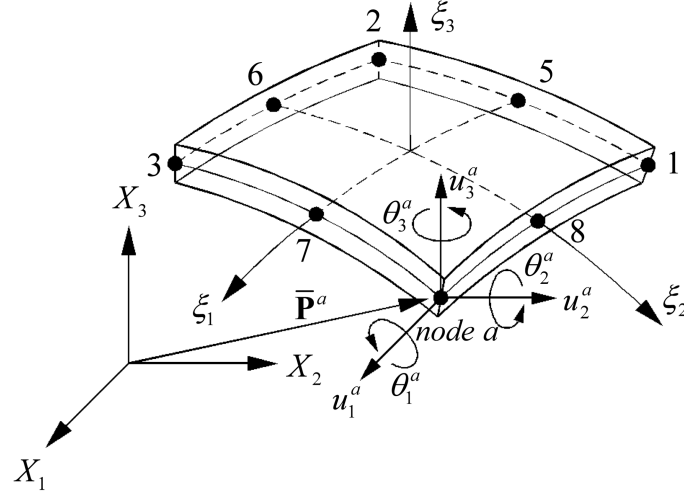
Fig. 1 Geometry of 8-node shell element with six degrees of freedom

and

$$\mathbf{u}(\xi_i) = \overline{\mathbf{u}}(\xi_j) + \xi_3\,\overline{\mathbf{e}}(\xi_j) + \xi_3^2\boldsymbol{\varphi}(\xi_j) + \xi_3^3\boldsymbol{\psi}(\xi_j) \quad ; \quad i = 1,2,3 \ , \quad j = 1,2 \tag{2}$$

where $\mathbf{P}$ denotes the position vector of a generic point in the shell element; $\overline{\mathbf{P}}$ and $\overline{\mathbf{V}}$ are the position vector of a point in the mid-surface and a normal vector to the mid-surface; $\overline{\mathbf{u}}$ and $\overline{\mathbf{e}}$ are the translational displacement vector and the fiber displacement vector respectively of a point in the mid-surface; $\boldsymbol{\Phi}$, $\boldsymbol{\Psi}$ and $\boldsymbol{\varphi}$, $\boldsymbol{\psi}$ are the corresponding higher order terms in $\mathbf{P}(\xi_i)$ and $\mathbf{u}(\xi_i)$ respectively.

It should be noted that the Green strain tensor and the natural strain have the following tensor transformation relationship

$$\tilde{E}_{\alpha\beta} = \frac{\partial \mathbf{P}_I}{\partial \xi_\alpha}\frac{\partial \mathbf{P}_J}{\partial \xi_\beta} E_{IJ}$$

$$= \frac{\partial \mathbf{P}_I}{\partial \xi_\alpha}\frac{\partial \mathbf{P}_J}{\partial \xi_\beta}\cdot\frac{1}{2}\left[\frac{\partial \mathbf{u}_I}{\partial \mathbf{P}_J} + \frac{\partial \mathbf{u}_J}{\partial \mathbf{P}_I} + \frac{\partial \mathbf{u}_K}{\partial \mathbf{P}_I}\frac{\partial \mathbf{u}_K}{\partial \mathbf{P}_J}\right]$$

$$= \frac{1}{2}\left[\frac{\partial \mathbf{P}_I}{\partial \xi_\alpha}\frac{\partial \mathbf{u}_I}{\partial \xi_\beta} + \frac{\partial \mathbf{u}_J}{\partial \xi_\alpha}\frac{\partial \mathbf{P}_J}{\partial \xi_\beta} + \frac{\partial \mathbf{u}_K}{\partial \xi_\alpha}\frac{\partial \mathbf{u}_K}{\partial \xi_\beta}\right] \tag{3}$$

By substituting Eq. (1) and Eq. (2) into Eq. (3), and remove the nonlinear terms, one can obtain

$$\tilde{E}_{\alpha\beta} = \frac{1}{2}\left[\frac{\partial(\overline{\mathbf{P}}_I + \xi_3\,\overline{\mathbf{V}}_I + \xi_3^2\boldsymbol{\Phi}_I + \xi_3^3\boldsymbol{\Psi}_I)}{\partial \xi_\alpha}\frac{\partial(\overline{\mathbf{u}}_I + \xi_3\,\overline{\mathbf{e}}_I + \xi_3^2\boldsymbol{\varphi}_I + \xi_3^3\boldsymbol{\psi}_I)}{\partial \xi_\beta}\right.$$
$$\left. + \frac{\partial()\overline{\mathbf{u}}_J + \xi_3\,\overline{\mathbf{e}}_J + \xi_3^2\boldsymbol{\varphi}_J + \xi_3^3\boldsymbol{\psi}_J}{\partial \xi_\alpha}\frac{\partial(\overline{\mathbf{P}}_J + \xi_3\,\overline{\mathbf{V}}_J + \xi_3^2\boldsymbol{\Phi}_J + \xi_3^3\boldsymbol{\Psi}_J)}{\partial \xi_\beta}\right] \tag{4}$$

The in-plane strains with the exception of the ξ_3^3 terms can represent the through thickness distribution with sufficient accuracy. Neglecting the higher-order terms in the general expression of the in-plane strains will result in identical form to the in-plane strain expressions based on the first-order theory. Then the transverse natural shear stains can be obtained as

$$\tilde{E}_{\alpha 3} = \frac{1}{2}\left[\frac{\partial \mathbf{P}_I}{\partial \xi_\alpha}\left(\overline{\mathbf{e}}_I + 2\xi_3 \boldsymbol{\varphi}_I + 3\xi_3^2 \boldsymbol{\psi}_I \right) + \frac{\partial \mathbf{u}_J}{\partial \xi_\alpha}\left(\overline{\mathbf{V}}_J + 2\xi_3 \boldsymbol{\Phi}_J + 3\xi_3^2 \boldsymbol{\Psi}_J \right) \right] \tag{5}$$

In view of the vanishing of the transverse natural shear stress at the top and bottom shell surfaces, i.e., $\tilde{S}_{23}(\pm 1) = \tilde{S}_{13}(\pm 1) = 0$, and the corresponding natural shear strains, the position vector, Eq. (1), and the displacement vector, Eq. (2) can be simplified into

$$\mathbf{P}(\xi_i) = \overline{\mathbf{P}}(\xi_j) + \xi_3\,\overline{\mathbf{V}}(\xi_j) + \xi_3^3\boldsymbol{\Psi}(\xi_j) = \overline{\mathbf{P}}(\xi_j) + \xi_3\left(1 - \frac{\xi_3^2}{3} \right)\overline{\mathbf{V}}(\xi_j) \tag{6}$$

$$\mathbf{u}(\xi_i) = \overline{\mathbf{u}}(\xi_j) + \xi_3\,\overline{\mathbf{e}}(\xi_j) + \xi_3^3\boldsymbol{\psi}(\xi_j) = \overline{\mathbf{u}}(\xi_j) + \xi_3\left(1 - \frac{\xi_3^2}{3} \right)\overline{\mathbf{e}}(\xi_j) \tag{7}$$

By substituting Eq. (6) and Eq. (7) into Eq. (5), the transverse natural shear strains can obtain

$$\tilde{E}_{\alpha 3}^s = \frac{1}{2}\left[\frac{\partial \mathbf{P}_I}{\partial \xi_\alpha}\frac{\partial\left(\overline{\mathbf{u}}_I + \xi_3\left(1 - \frac{\xi_3^2}{3} \right)\overline{\mathbf{e}}_I \right)}{\partial \xi_3} + \frac{\partial \mathbf{u}_J}{\partial \xi_\alpha}\frac{\partial\left(\overline{\mathbf{P}}_J + \xi_3\left(1 - \frac{\xi_3^2}{3} \right)\overline{\mathbf{V}}_J \right)}{\partial \xi_3} \right]$$

$$= \frac{1}{2}\left[\frac{\partial \mathbf{P}_I}{\partial \xi_\alpha}\overline{\mathbf{e}}_I + \frac{\partial \mathbf{u}_J}{\partial \xi_\alpha}\overline{\mathbf{V}}_J \right](1 - \xi_3^2) \tag{8}$$

The transverse natural shear strains in Eq. (8) are identical to those in the first-order shear deformation theory if the ξ_3^2 term is excluded. Accordingly, the combination of the transverse natural shear strains in the first-order shear deformation theory and Eq. (8) results in a parabolic through-thickness distribution for the transverse natural shear strains and satisfies the zero transverse shear stress requirement at the shell surfaces. Thus, it eliminates the need for the shear correction factors in the first-order theory. Finally, the ratio, h_ξ of effective transverse shear energy U_s to the average transverse shear energy $\overline{U}_s$ can be determined. In this paper, we present, in brief, the more general case of multilayer laminated composite plates where stresses are not continuous across the inter-lamina boundaries.

Assume that the effective magnitudes of transverse shear stress and shear strains are denoted as $\tilde{S}_{\alpha 3}^e$ and $\tilde{E}_{\alpha 3}^e$, respectively, the actual transverse shear stress and strain through the thickness are expressed accordingly as

$$\tilde{S}_{\alpha 3}^s = \tilde{S}_{\alpha 3}^e(\xi_1)H_\tau(\xi_3) \tag{9a}$$

$$\tilde{E}_{\alpha 3}^s = \tilde{E}_{\alpha 3}^e(\xi_1)H_\gamma(\xi_3) \tag{9b}$$

where $H_\tau(\xi_3)$ and $H_\gamma(\xi_3)$ are distribution shape function of transverse shear stress and strain,

respectively (Qi *et al.* 1996). For isotropic plates and shells, $H_\tau(\xi_3)$ and $H_\gamma(\xi_3)$ take a special parabolic form.

The transverse shear energy U_s through the thickness is expressed as

$$U_s = \frac{1}{2}\int \tilde{S}_{\alpha3}^s \tilde{E}_{\alpha3}^s d\xi_3 = \frac{1}{2}\tilde{S}_{\alpha3}^e \tilde{E}_{\alpha3}^e \int H_\tau(\xi_3) H_\gamma(\xi_3) d\xi_3 \tag{10}$$

On the other hand, the transverse shear strain energy can also be expressed in terms of the average shear strain. Namely

$$\bar{U}_s = \frac{1}{2}\bar{E}_{\alpha3}\int \tilde{S}_{\alpha3}^s d\xi_3 = \frac{1}{2}\bar{E}_{\alpha3}\tilde{S}_{\alpha3}^e \int H_\tau(\xi_3) d\xi_3 \tag{11}$$

Equating these two transverse shear strain energy expressions ($U_s = \bar{U}_s$) and solving for the nominal uniform transverse shear strain $\bar{E}_{\alpha3}^e$ give

$$\bar{E}_{\alpha3}^e = \frac{\int \tilde{S}_{\alpha3}^s \tilde{E}_{\alpha3}^s d\xi_3}{\int \tilde{S}_{\alpha3}^s d\xi_3} = \frac{\int H_\tau(\xi_3) H_\gamma(\xi_3) d\xi_3}{\int H_\tau(\xi_3) d\xi_3}\tilde{E}_{\alpha3}^e \tag{12}$$

Alternatively, the ratio of transverse shear strain effective magnitude $\bar{E}_{\alpha3}^e$ to the nominal uniform shear strain $\bar{E}_{\alpha3}^e$ is

$$h_\xi = \frac{\tilde{E}_{\alpha3}^e}{\bar{E}_{\alpha3}} = \frac{\int H_\tau(\xi_3) d\xi_3}{\int H_\tau(\xi_3) H_\gamma(\xi_3) d\xi_3} \tag{13}$$

The refined first-order shear deformation theory can then be presented as a function of $(1-\xi_3^2)$ and h_ξ factorizing the transverse shear strains in the first-order shear deformation theory as follows

$$\tilde{E}_{\alpha3}^s = \tilde{E}_{\alpha3}^e \cdot H_\gamma(\xi_3) = \bar{E}_{\alpha3} \cdot H_\gamma(\xi_3) \cdot h_\xi = \frac{1}{2}\left[\frac{\partial \mathbf{P}_I}{\partial \xi_\alpha}\bar{\mathbf{e}}_I + \frac{\partial \mathbf{u}_J}{\partial \xi_\alpha}\bar{\mathbf{V}}_J\right](1-\xi_3^2)h_\xi \tag{14}$$

With the displacement fields and stress-strain relationships defined as above, the membrane and shear forces and bending moments can be evaluated from the constitutive equations. For single layer plates and shells, these equations are quite straightforward. The membrane forces, the bending moments and the transverse shear forces can be obtained by integrating the relevant stresses through the thickness using the equivalent constitutive equations

$$\begin{Bmatrix} \mathbf{R}_{mb} \\ \mathbf{R}_s \end{Bmatrix} = \begin{bmatrix} \mathbf{D}_{mb} & 0 \\ 0 & \mathbf{D}_s \end{bmatrix} \begin{Bmatrix} \tilde{\mathbf{e}}^{mb} \\ \tilde{\mathbf{e}}^s \end{Bmatrix} \tag{15}$$

where $\mathbf{R}_{mb} = \{\mathbf{N}_{\xi_1}, \mathbf{N}_{\xi_2}, \mathbf{N}_{\xi_1\xi_2}, \mathbf{M}_{\xi_1}, \mathbf{M}_{\xi_2}, \mathbf{M}_{\xi_1\xi_2}\}$ and $\mathbf{R}_s = \{\mathbf{Q}_{\xi_1}, \mathbf{Q}_{\xi_2}\}$.

The matrix sizes of the membrane-bending rigidity $\mathbf{D}_{mb}$ and shear strain rigidity $\mathbf{D}_s$ are 6 × 6 and 2 × 2 respectively. They can be evaluated as follows

$$\mathbf{D}_{mb} = \int_{-h/2}^{h/2} \begin{bmatrix} \mathbf{C}_1 & \xi_3\mathbf{C}_1 \\ \xi_3\mathbf{C}_1 & \xi_3^2\mathbf{C}_1 \end{bmatrix} d\xi_3 \tag{16}$$

where $\mathbf{C}_1$ is the elastic constitutive coefficient, and

$$\mathbf{D}_s = \int_{-h/2}^{h/2} \begin{bmatrix} G & 0 \\ 0 & G \end{bmatrix} \left(1 - \xi_3^2\right) h_\xi \, d\xi_3 \tag{17}$$

When the entire cross section is homogeneous, the rigidity matrix reduces to the following form

$$\mathbf{D}_e = \begin{bmatrix} h\mathbf{C}_1 & 0 & 0 \\ 0 & \dfrac{h^3}{12}\mathbf{C}_1 & 0 \\ 0 & 0 & h\mathbf{C}_2 \end{bmatrix} \tag{18}$$

where $\mathbf{C}_1$ and $\mathbf{C}_2$ are the elastic constitutive coefficients of the membrane-bending and the transverse shear components.

3. Various enhanced strain interpolation patterns

The 8-node shell elements have been studied in various papers (Hinton and Huang 1986, Lakshinarayanan *et al.* 1989, Macneal and Harder 1992, Bucalem and Bathe 1993, Kim *et al.* 2002, 2003). For the new efficient 8-node shell element, the usual 8-nodes of Lagrangian displacement interpolations are employed and the various combinations of assumed natural strain interpolation functions are used. Fig. 2 lists various patterns of sampling points that can be employed for membrane, in-plane shear and transverse shear strain interpolations for the new 8-node shell element. Based on Fig. 2, the α pattern is used for membrane ($\alpha\delta\beta$ and $\alpha\delta\gamma$) and the β pattern is used for membrane ($\beta\delta\gamma$) as well as transverse shear ($\alpha\delta\beta$). The δ pattern and γ pattern are used for in-plane and transverse shear, respectively.

The interpolation functions by Huang (1989) are used in the γ pattern. The three cases of the combinations of various sampling points are used in the analysis.

4. Equilibrium equation

Using virtual work principle, the following equilibrium equation is obtained based on the membrane, bending and transverse shear resultant forces as follows

$$\int (\delta(\tilde{E}_{\alpha\beta}^m)^T \mathbf{N} + \delta(\tilde{E}_{\alpha\beta}^b)^T \mathbf{M} + \delta(\tilde{E}_{\alpha3}^s)^T \mathbf{Q}) \, dA \equiv \delta \mathbf{u}^T \mathbf{K}_L \mathbf{u} = \int \mathbf{f} \cdot \delta \mathbf{u} \, dV \tag{19}$$

where $\tilde{E}_{\alpha\beta}^m, \tilde{E}_{\alpha\beta}^b, \tilde{E}_{\alpha3}^s$ are membrane, bending and transverse shear strain components and $\mathbf{f}$ is the body force.

If we consider only the linear component in Eq. (19), the linear stiffness matrix can be evaluated as $\mathbf{K}_L$ (Han *et al.* 2004).

The element stiffness matrix may be written in a matrix form using the equivalent constitutive equations. Finally the element stiffness matrix has 6×6 size on the reference-surface of shell element. The torsional stiffness term was formed as described by Kanok-Nukulchai (1979) and added to the stiffness term.

(a) Pattern α (b) Pattern β

(following Bathe *et al.* 2003)

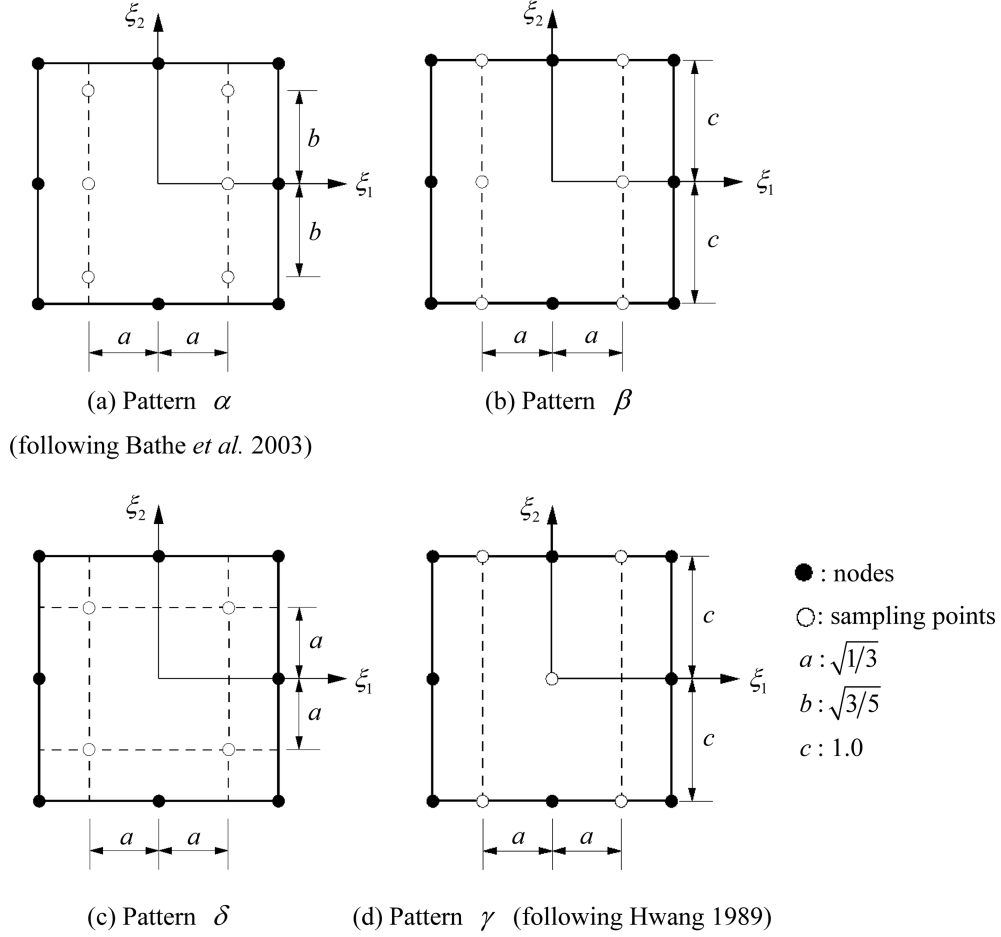(c) Pattern δ (d) Pattern γ (following Hwang 1989)

Fig. 2 Four possible pattern of sampling points for 8-node ANS shell element

5. Torsional effect

In this study, based on the procedure proposed by Kanok-Nukulchai (1979), the drilling degree of freedom will be tied to the in-plane twist by a penalty functional through an additional artificial strain energy as

$$U_t = k_t G \int_{V^e} \left[\alpha_t(\xi_1, \xi_2) - \frac{1}{2} \left\{ \frac{\partial w_2}{\partial z_1}(\xi_1, \xi_2, 0) - \frac{\partial w_1}{\partial z_2}(\xi_1, \xi_2, 0) \right\} \right]^2 dV \qquad (20)$$

where k_t is a parameter to be determined (the value of 0.1 suggested); G is the shear modulus; V^e is the volume of the element; and dV is the volume element. After integration throughout the thickness, Eq. (20) can be written as

$$U_t = k_t G h \int_{S^e} \left[\alpha_t(\xi_1, \xi_2) - \frac{1}{2} \left\{ \frac{\partial w_2}{\partial z_1}(\xi_1, \xi_2, 0) - \frac{\partial w_1}{\partial z_2}(\xi_1, \xi_2, 0) \right\} \right]^2 d\xi_1 d\xi_2 \qquad (21)$$

If k_tGh is chosen to be large relative to the factor Eh^3 (which appears in the bending energy), Eq. (21) will play the role of penalty function and result in the desired constraint

$$\alpha_t(\xi_1,\xi_2) \approx \frac{1}{2}\left\{\frac{\partial w_2}{\partial z_1}(\xi_1,\xi_2,0) - \frac{\partial w_1}{\partial z_2}(\xi_1,\xi_2,0)\right\} \qquad (22)$$

at the Gauss points. A two-by-two Gauss integration scheme is applied for the evaluation of the torsional stiffness in order to avoid the over-constrained situation. To derive a torsional stiffness from Eq. (21) the local variables are expressed in terms of global nodal variables, $\mathbf{u}$, by shape functions. This gives Eq. (21) in the form (Kanok-Nukulchai 1979)

$$U_t = \mathbf{u}^T \mathbf{K}_{tL} \mathbf{u} \qquad (23)$$

The torsional stiffness term $\mathbf{K}_{tL}$ is added as described by Kanok-Nukulchai (1979).

6. Numerical results of the 8-node shell element

Several numerical examples are solved to test the performance of the shell element in linear applications. The patch test, distortion test and other various numerical tests of the present shell elements are carried out and validated using FEAP program (Zienkiewicz and Taylor 1989, 2000). The present shell element shows excellent performance in agreement with references. Several examples demonstrate the efficiency and accuracy of the present shell element. Note that most of the results presented here are normalized with the reference solution.

6.1 Patch test

In the study the basic patch tests proposed by Simo *et al.* (1989) were performed and the results illustrated in Fig. 3. A patch of five elements is used is this study. Boundary and loading conditions

Table 1 List of shell elements used for comparison

Name	DESCRIPTION (Patterns referred to Fig. 2)
Present ($\alpha\delta\beta$)	Sampling points for membrane (Pattern α), in-plane shear (Pattern δ) and transverse shear (Pattern β).
Present ($\alpha\delta\gamma$)	Sampling points for membrane (Pattern α), in-plane shear (Pattern δ) and transverse shear (Pattern γ).
Present ($\beta\delta\gamma$)	Sampling points for membrane (Pattern β), in-plane shear (Pattern δ) and transverse shear (Pattern γ).
QUAD8	8-node shell element(Selective Integration) (MacNeal and Harder 1989)
QUAD8*	8-node shell element (STRAND 7 2000)
QUAD8**	8-node ANS shell element (Lakshminarayana and Kailash 1989)
XSHELL41	4-node quasi-conforming shell element (Kim *et al.* 2003)
XSHELL-8-ANS	8-node assumed natural strain shell element (XFINAS 2008)
MITC8	8-node shell element using a mixed interpolation of tensorial components (Bathe and Dvorkin 1986)

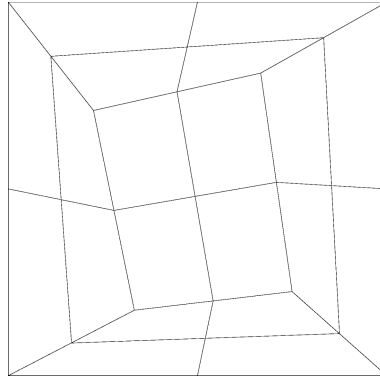Fig. 3 Mesh for patch test (Simo *et al.* 1989). Length of the square $L = 10$; Young's modulus $E = 1.0 \times 10^{7}$; Posson's ratio $\nu = 0.3$; and thickness $h = 1.0$

(a) Bending test

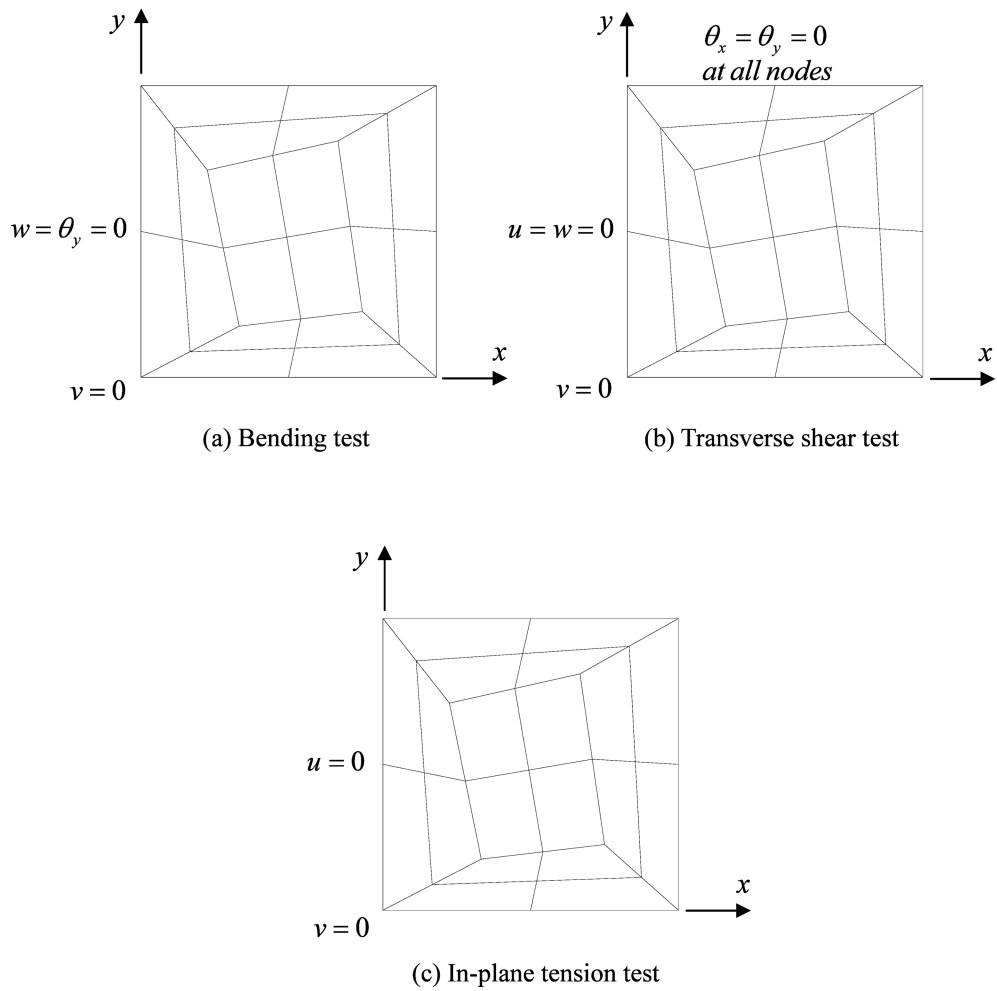(b) Transverse shear test

(c) In-plane tension test

Fig. 4 Boundary displacement conditions for patch tests

are illustrated in Figs. 4 and 5, respectively. Tables 2-4 present the normalized solutions of nodal displacements on the right edges. The normalized solutions are presented in the non-dimensional form using the equation

$$\text{Normalized solution} = \frac{\text{Present solution}}{\text{Reference solution}} \qquad (24)$$

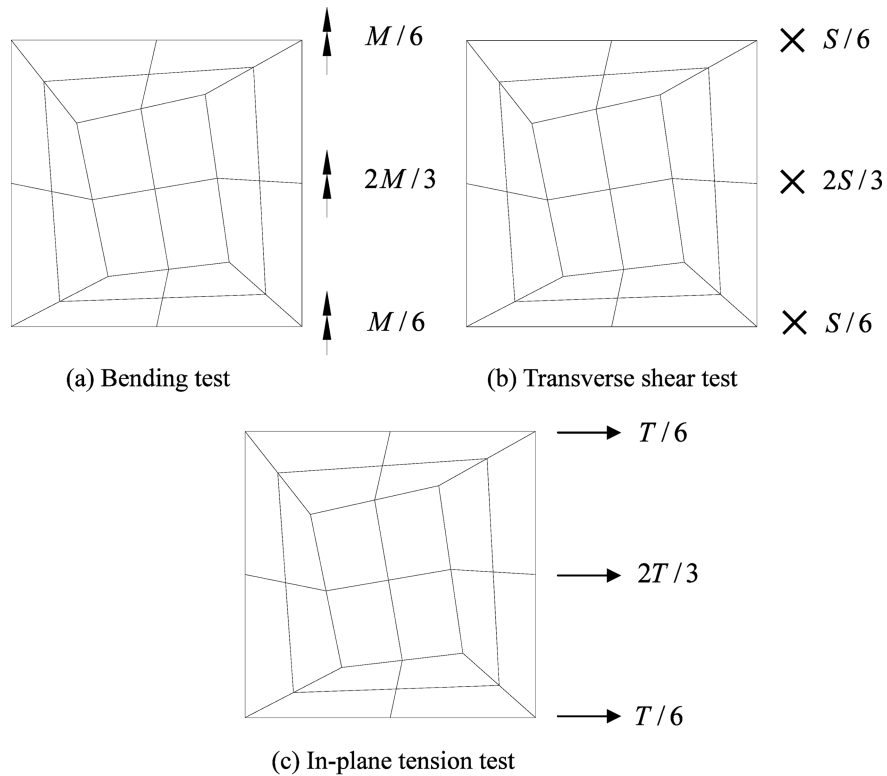(a) Bending test   (b) Transverse shear test

(c) In-plane tension test

Fig. 5 Loading conditions for patch tests

Table 2 Results of patch test under Bending (Reference solution : $\theta_y = ML/EI = 0.12 \times 10^{-4}$)

Combinations of Various Sampling Points	$\alpha\delta\beta$	$\alpha\delta\gamma$	$\beta\delta\gamma$
Normalized Solutions	1.000	1.000	1.000

Table 3 Results of patch test under out-of-plane shear (Reference solution : $w = 6SL/5GA = 0.312 \times 10^{-5}$)

Combinations of Various Sampling Points	$\alpha\delta\beta$	$\alpha\delta\gamma$	$\beta\delta\gamma$
Normalized Solutions	0.053	0.989	0.989

Table 4 Results of patch test under in-plane tension (Reference solution : $u = TL/EA = 1.0 \times 10^{-6}$)

| Combinations of Various Sampling Points	$\alpha\delta\beta$	$\alpha\delta\gamma$	$\beta\delta\gamma$
Normalized Solutions	1.000	0.965	0.992

Patch test results indicate that various sampling points for assumed natural strain method in Tables 2-4 can represent fields of constant moment, constant in-plane tension, transverse shear forces. The present shell element can pass the patch test when patterns $\alpha\delta\gamma$ and $\beta\delta\gamma$ are used in all cases, and pass the patch test approximately when pattern $\alpha\delta\beta$ is used in pure transverse shear case. Therefore, we found that it is very important to apply the best combination of sampling points for 8-node shell elements.

6.2 Cantilever beam problem

6.2.1 Straight beam problem

MacNeal and Harder (1985) suggested three separate cantilever beam tests that evaluate sensitivity to various deformation patterns and distortions of the element geometry, i.e., a) a straight beam, b) a curved beam and c) a twisted beam. Descriptions of the straight, curved and twisted beam problems are provided in Figs. 6-8. Normalized tip displacements in direction of load are presented in Tables 5-20. Reference solutions (MacNeal and Harder 1985) are also given in Tables 5-20.

The straight cantilever beam is a frequently used test problem which can be modeled as beam, plate, and solid elements. Its virtues are its simplicity and the fact that all of the principal element deformation modes described earlier can be evoked by loads applied to the free end, including extension, in-plane shearing, out-of-plane shearing and twisting. In this study, irregular elements shapes are added to test the accuracy of shell elements.
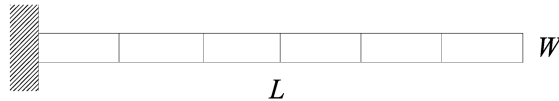
$E = 1.0 \times 10^7$, $\quad v = 0.3$, $\quad L = 6.0$, $\quad W = 0.2$, $\quad h = 0.1$, Loading : unit forces at free end

Fig. 6 Straight beam problem

a) Rectangular elements

Table 5 Results of straight beam ($h = 0.1$) under extension (Reference solution : $u = 3.0 \times 10^{-5}$)

Element Size	Normalized Solutions				
	$\alpha\delta\beta$	$\alpha\delta\gamma$	$\beta\delta\gamma$	QUAD8	QUAD8**
6 × 1	0.998	0.998	0.998	0.999	0.998

Table 6 Results of straight beam ($h = 0.1$) under in-plane shear (Reference solution : $v = 0.1081$)

Element Size	Normalized Solutions				
	$\alpha\delta\beta$	$\alpha\delta\gamma$	$\beta\delta\gamma$	QUAD8	QUAD8**
6 × 1	0.986	0.986	0.986	0.987	0.985

Table 7 Results of straight beam (h = 0.1) under out-of-plane shear (Reference solution : w = 0.4321)

Element Size	Normalized Solutions				
	$\alpha\delta\beta$	$\alpha\delta\gamma$	$\beta\delta\gamma$	QUAD8	QUAD8**
6 × 1	0.990	0.994	0.994	0.991	0.996

Table 8 Results of straight beam (h = 0.1) under twist shear (Reference solution : θ_x = 0.03208)

Element Size	Normalized Solutions				
	$\alpha\delta\beta$	$\alpha\delta\gamma$	$\beta\delta\gamma$	QUAD8	QUAD8**
6 × 1	0.946	0.945	0.945	0.950	0.944

b) Trapezoidal elements

Table 9 Results of straight beam (h = 0.1) under extension (Reference solution : u = 3.0 × 10^{-5})

Element Size	Normalized Solutions				
	$\alpha\delta\beta$	$\alpha\delta\gamma$	$\beta\delta\gamma$	QUAD8	QUAD8**
6 × 1	0.998	0.969	0.971	0.999	0.998

Table 10 Results of straight beam (h = 0.1) under in-plane shear (Reference solution : v = 0.1081)

Element Size	Normalized Solutions				
	$\alpha\delta\beta$	$\alpha\delta\gamma$	$\beta\delta\gamma$	QUAD8	QUAD8**
6 × 1	0.896	0.893	0.890	0.946	0.906

Table 11 Results of straight beam (h = 0.1) under out-of-plane shear (Reference solution : w = 0.4321)

Element Size	Normalized Solutions				
	$\alpha\delta\beta$	$\alpha\delta\gamma$	$\beta\delta\gamma$	QUAD8	QUAD8**
6 × 1	fail	0.993	0.993	0.998	0.995

Table 12 Results of straight beam (h = 0.1) under twist shear (Reference solution : θ_x = 0.03208)

Element Size	Normalized Solutions				
	$\alpha\delta\beta$	$\alpha\delta\gamma$	$\beta\delta\gamma$	QUAD8	QUAD8**
6 × 1	fail	0.941	0.941	0.887*	0.944

*MacNeal and Harder (1992)

c) Parallelogram elements

Table 13 Results of straight beam (h = 0.1) under extension (Reference solution : u = 3.0 × 10^{-5})

Element Size	Normalized Solutions				
	$\alpha\delta\beta$	$\alpha\delta\gamma$	$\beta\delta\gamma$	QUAD8	QUAD8**
6 × 1	0.998	0.999	1.000	0.999	0.998

Table 14 Results of straight beam (h = 0.1) under in-plane shear (Reference solution : v = 0.1081)

Element Size	Normalized Solutions				
	$\alpha\delta\beta$	$\alpha\delta\gamma$	$\beta\delta\gamma$	QUAD8	QUAD8**
6 × 1	0.979	0.988	0.984	0.995	0.965

Table 15 Results of straight beam (h = 0.1) under out-of-plane shear (Reference solution : w = 0.4321)

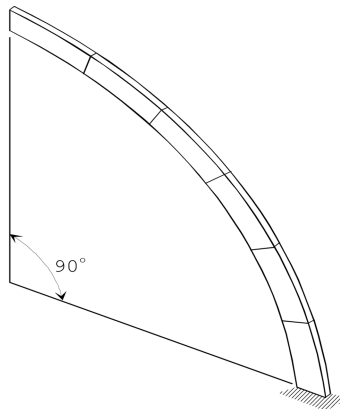| Element Size	Normalized Solutions				
	$\alpha\delta\beta$	$\alpha\delta\gamma$	$\beta\delta\gamma$	QUAD8	QUAD8**
6 × 1	fail	0.993	0.993	0.985	0.991

Table 16 Results of straight beam (h = 0.1) under twist shear (Reference solution : θ_x = 0.03208)

Element Size	Normalized Solutions				
	$\alpha\delta\beta$	$\alpha\delta\gamma$	$\beta\delta\gamma$	QUAD8	QUAD8**
6 × 1	fail	0.945	0.945	0.965	0.891

Good performance of the present element is observed in all cases except the case of $\alpha\delta\beta$ under out-of-plane and twist shear with irregular elements. Thus, the β pattern does not seem to be suitable for the transverse shear strains because of the locking phenomenon of straight beams under out-of-plane and twist shear.

6.2.2 Curved beam problem

In the curved cantilever beam, combination of the principal deformation modes is evoked by a single in-plane or an out-of-plane shear load at the free end. Note also that the element shape is quite rectangular, which will test the effect of slight irregularity. MacNeal and Harder (1985) suggested a reference solution of 0.08734 as a theoretical displacement at the loading point. A different solution of 0.08854 was given by Young (1989).

$R_i = 4.12, R_e = 4.32, arc = 90°, E = 1 \times 10^7, v = 0.25, h = 0.1,$

Loading : unit forces at free end

Fig. 7 Curved cantilever beam

Table 17 Results of curved beam (h = 0.1) under in-plane shear (Reference solution[a] : v = 0.08854)

Element Size	Normalized Solutions				
	$\alpha\delta\beta$	$\alpha\delta\gamma$	$\beta\delta\gamma$	QUAD8*	QUAD8**
6 × 1	0.991	0.991	0.991	0.869	0.942

[a]From (Young 1989)

Table 18 Results of curved beam (h = 0.1) under out-of-plane shear (Reference solution[a] : w = 0.5022)
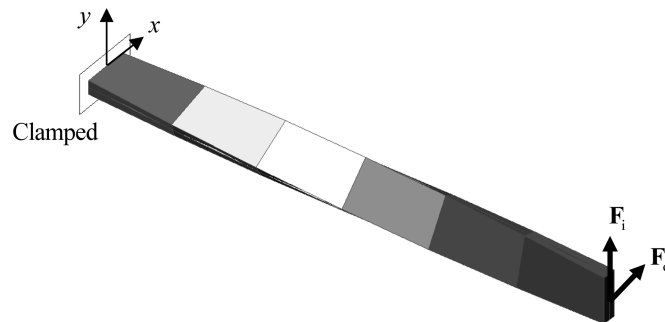
Element Size	Normalized Solutions				
	$\alpha\delta\beta$	$\alpha\delta\gamma$	$\beta\delta\gamma$	QUAD8*	QUAD8**
6 × 1	0.970	0.970	0.970	0.958	0.962

[a]From (MacNeal and Harder 1985)

Results presented in Tables 17-18 show the outstanding performance of the proposed element.

6.2.3 Twisted beam problem

The twisted beam problem (shown in Fig. 8), which was introduced by MacNeal and Harder (1985), was proposed to test the effect of element warping. The performance of elements of thickness (0.32) was investigated under in-plane and out-of-plane shear loads. The warp of each element is 15°. Numerical results in Tables 19-20 are listed with displacements of free end normalized to the reference solution. Reference solutions (MacNeal and Harder 1985) are also given in Tables 19-20.

Length=12, Width=1.1, Twist = $90°$, $E = 29 \times 10^6$, $v = 0.22$, $h = 0.32$,

Loading : unit forces at free end

Fig. 8 Twisted cantilever beam

Table 19 Results of twisted beam (h = 0.32) under in-plane shear (Reference solution : v = 5.424 × 10^{-3})

Element Size	Normalized Solutions				
	$\alpha\delta\beta$	$\alpha\delta\gamma$	$\beta\delta\gamma$	QUAD8	QUAD8**
6 × 1	0.988	0.996	0.997	0.998 (12 × 2)	0.998 (12 × 2)

Table 20 Results of twisted beam (h = 0.32) under out-of-plane shear (Reference solution : u = 1.754 × 10^{-3})

Element Size	Normalized Solutions				
	$\alpha\delta\beta$	$\alpha\delta\gamma$	$\beta\delta\gamma$	QUAD8	QUAD8**
6 × 1	0.995	1.000	1.001	0.998 (12 × 2)	0.998 (12 × 2)
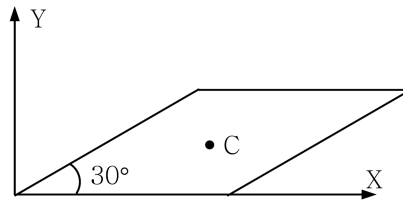
$Length = 100, E = 1.0 \times 10^6, v = 0.3, h = 1.0, Uniform\ Load = 1.0$

Fig. 9 Rhombic plate under uniform pressure

Table 21 Results of rhombic plate (w_C = 0.04640)

Element Size	Normalized Solutions				
	$\alpha\delta\beta$	$\alpha\delta\gamma$	$\beta\delta\gamma$	XSHELL-8-ANS	QUAD8**
4 × 4	0.519	0.838	0.838	0.519	0.440
8 × 8	0.745	0.886	0.886	0.745	0.710
16 × 16	0.874	0.947	0.947	0.874	0.873 (12 × 12)

Results are presented in Tables 19-20, showing more correct results in spite of (6 × 1) mesh.

6.3 Bending of rhombic plate

A simply supported rhombic plate in Fig. 9 is subjected to a uniformly distributed load. This is rather a challenging test due to the singularity of its solution at the obtuse vertices. The numerical results for the center deflection are presented in Table 21 with those from several existing elements. The reference solution was u_C = 0.04640 proposed by Andelfinger and Ramm (1993).
Very good results are obtained with the present element as well as the QUAD8** element.

6.4 Bending of rectangular plate

The simply supported and clamped rectangular plate problem under uniform and central point loading is applied to test shear locking by changing of aspect ratios. Two aspect ratios of b/a = 1 and 5 were considered, and a quarter was modeled due to symmetry. To test the general applicability, the plate is analyzed using both a rectangular mesh and a distorted mesh. Reference solutions (MacNeal and Harder 1985) are given in Tables 22-27.
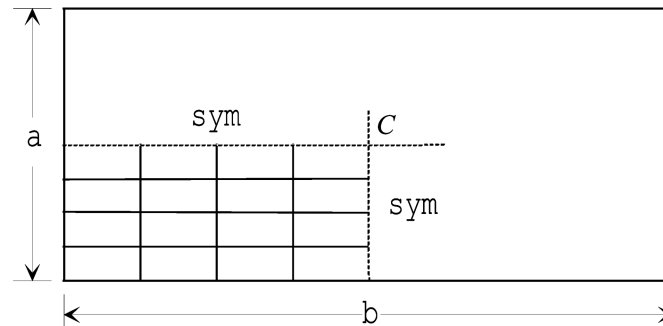
$$a = 2.0, b = 2.0, 10.0, E = 1.7472 \times 10^7, v = 0.3, h = 0.0001,$$

Concentrated load at center = 4.0×10^4 or Uniform load = 1.0.

Fig. 10 Simply supported and clamped rectangular plate

6.4.1 Rectangular mesh

(a) For the case of *b/a* = 1.0

The reference vertical deflection at the center of the simply supported plate under uniform load is 4.062 and the clamped plate under concentrated load is 5.60. In Tables 22 and 23, the numerical results obtained by using different types of existing elements are listed.

(1) Simply supported plate – Uniform load

Table 22 Results of rectangular plate (*b/a* = 1.0; Reference solution : w_C = 4.062)

Element Size	Normalized Solutions				
	$\alpha\delta\beta$	$\alpha\delta\gamma$	$\beta\delta\gamma$	QUAD8	QUAD8**
4 × 4	Locking	1.009	1.009	1.000	1.016

(2) Clamped plate – Concentrated load

Table 23 Results of rectangular plate (*b/a* = 1.0; Reference solution : w_C = 5.60)

Element Size	Normalized Solutions				
	$\alpha\delta\beta$	$\alpha\delta\gamma$	$\beta\delta\gamma$	QUAD8	QUAD8**
4 × 4	0.123	1.057	1.057	0.997	1.090

(b) For the case of *b/a* = 5.0

The reference deflection at the center of the simply supported plate under uniform load is 12.97 and the clamped plate under concentrated load is 7.23. In Tables 24 and 25, the numerical results obtained by using different types of elements are listed.

(1) Simply supported plate – Uniform load

Table 24 Results of rectangular plate (b/a = 5.0; Reference solution : w_C = 12.97)

Element Size	Normalized Solutions				
	$\alpha\delta\beta$	$\alpha\delta\gamma$	$\beta\delta\gamma$	QUAD8	QUAD8**
4 × 4	Locking	1.009	1.009	1.000	1.010

(2) Clamped plate – Concentrated load

Table 25 Results of rectangular plate (b/a = 5.0; Reference solution : w_C = 7.23)

Element Size	Normalized Solutions				
	$\alpha\delta\beta$	$\alpha\delta\gamma$	$\beta\delta\gamma$	QUAD8	QUAD8**
4 × 4	0.129	0.845	0.845	0.975	0.867
8 × 4	Locking	1.029	1.029	-	-

Locking problems occurred when the β pattern is applied to transverse shear strain in thin plates. This particular example shows the limit of 8-node shell element for the application of β pattern. Because other cases still have the errors, a specifically designed application must be developed in order to remove these errors in the present shell element.

6.4.2 Distorted mesh
(a) For the case of *b/a* = 1.0
To test the general applicability of the present formulation for bending, a thin square plate, L/h = 20000 is analyzed using both a rectangular mesh and a distorted mesh. A clamped boundary condition is chosen because it is considered to be more severe compared to simple supports. Two types of loading are considered, concentrated load and distributed load. Geometry and material
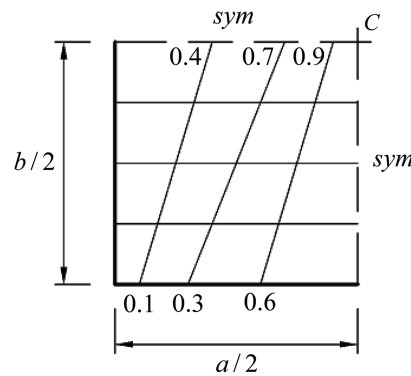
$a = 2.0, b = 2.0, E = 1.7472 \times 10^7, v = 0.3, h = 0.0001$

Fig. 11 Distorted mesh of simply supported and clamped rectangular plate

(1) Simply supported plate – Uniform and Concentrated load at center

Table 26 Results of Simply supported Plate with Rectangular and Distorted meshes (Reference solutions : $w_C = 4.062$ and 11.60)

Mesh types	Element	Uniform Load $(w_C = 4.062)$	Concentrated Load $(w_C = 11.60)$
Rectangular mesh	$\beta\delta\gamma$	1.009	1.022
Distorted mesh	$\beta\delta\gamma$	1.010	1.016

(2) Clamped plate – Uniform and Concentrated load at center

Table 27 Results of Clamped Plate with Rectangular and Distorted meshes (Reference solutions : $w_C = 1.2637$ and 5.60)

Mesh types	Elements	Uniform Load $(w_C = 1.2637)$	Concentrated Load $(w_C = 5.60)$
Rectangular mesh	Choi *et al.* (1999)*	0.965	0.990
	XSHELL41	0.997	0.992
	$\beta\delta\gamma$	1.052	1.057
Distorted mesh	Choi *et al.* (1999)*	0.976	1.011
	XSHELL41	1.023	0.995
	$\beta\delta\gamma$	1.049	1.039

*Results of Choi e*t al.* (1999) and XSHELL41 are referenced from Kim *et al.* (2003).

properties are provided in Fig. 11. A four by four mesh is used on one quarter of the plate. The results are compared in Tables 26 and 27 with those provided by Timoshenko and Woinowsky-Krieger (1959). The accuracy of the results obtained in both cases is maintained and compared with Choi *et al.* (1999) and Kim *et al.* (2003).

The reference vertical deflection at the center of the plate is the simply supported plate under uniform load is 4.062 and the clamped plate under concentrated load is 5.60. In Tables 26 and 27, the numerical results obtained by using different types of existing elements are listed.

The case of $\beta\delta\gamma$ is compared for the test of distorted mesh. It is also found that the locking phenomenon does not happen and the solutions with rectangular mesh are of similar accuracy.

6.5 Pinched hemispherical shell

The problem consists of a hemispherical shell with two inward and two outward forces that are 90° apart. There are two issues that are crucial for an element to yield good results in this problem. Firstly, an inextensional-bending mode must be allowed; and secondly, rigid-body motion must be well expressed. Two versions of this problem were considered: hemispherical shell with 18° hole and full hemispherical shell.

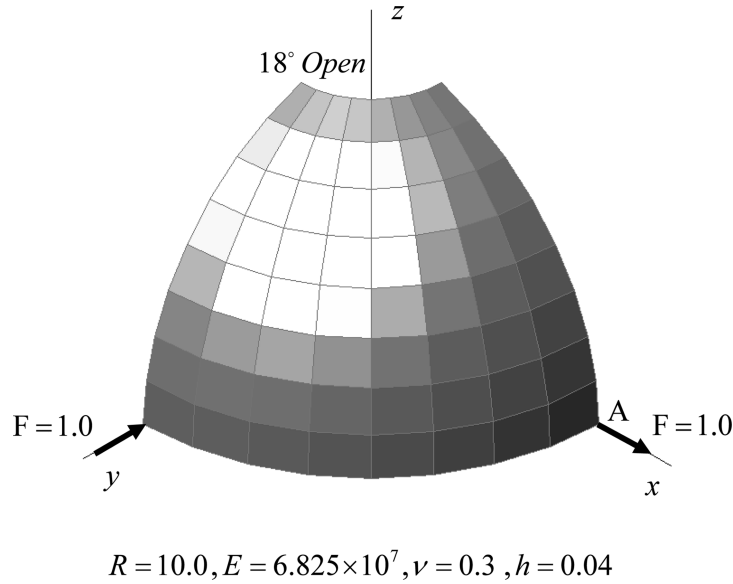$$R = 10.0, E = 6.825 \times 10^7, v = 0.3, h = 0.04$$

Fig. 12 Definition of loading points and initial configuration of hemispherical shell

Table 28 Results of hemispherical shell with 18× hole ($u_A = 0.093$)

Element Size	Normalized Solutions				
	$\alpha\delta\beta$	$\alpha\delta\gamma$	$\beta\delta\gamma$	QUAD8	QUAD8**
4 × 4	0.450	0.535	0.542	0.832	0.387
6 × 6	0.872	0.914	0.915	1.003	0.773
8 × 8	0.967	0.984	0.984	C*	0.950

*The grade C means that the QUAD8 gives accuracy 20% > error > 10%.
(MacNeal and Harder 1985)

For this problem, the reference deflection at point A in the *x*-direction is 0.093 (Simo *et al.* 1989). The geometry and material properties are shown in Fig. 12. The numerical results are given in Table 28.

We see that the results obtained by our elements are more accurate than the solution by the QUAD8** element. Note that the error of 8 × 8 mesh for the QUAD8 element is > 10%.

(b) Full hemispherical shell

Meshes for full hemispherical shell are highly skewed if few elements are used. In the present study, a quarter of the shell was divided into three equal parts, each of which was then modeled with the same element layout. The geometry and the material properties are shown in Fig. 13, while the numerical results are presented in Table 29. The reference deflection at point A in the *x*-direction is 0.0924 (Simo *et al.* 1989).
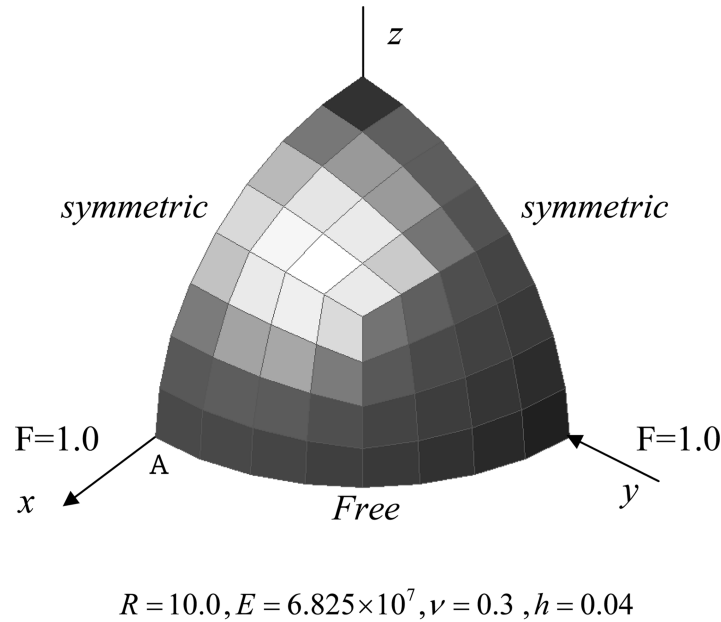
$$R = 10.0, E = 6.825 \times 10^7, v = 0.3, h = 0.04$$

Fig. 13 Pinched full hemispherical shell

Table 29 Results of Full Hemispherical Shell (u_A = 0.0924)

Nodes per Side	Normalized Solutions				
	$\alpha\delta\beta$	$\alpha\delta\gamma$	$\beta\delta\gamma$	XSHELL-8-ANS	QUAD8*
9	0.370	0.462	0.464	0.373	0.519
17	0.934	0.963	0.963	0.934	0.938

We see that our elements are more accurate than the reference element XSHELL-8-ANS. It was also found that the solutions with QUAD8* are of similar accuracy.

6.6 Scordelis-Lo roof problem

Both membrane and bending deformations are important for the solution of the Scordelis-Lo roof problem shown in Fig. 14. This problem can be used to determine the capability of the element in modeling membrane states in curved shells. This type of the problem was proposed by MacNeal and Harder (1985), who suggested a reference solution 0.3024 for the displacement at the point A. A different 'deep shell solution' of 0.3008 was given by Saleeb *et al.* (1987). Because of symmetry, only one quarter of the problem is modeled.

For this problem, the present element is clearly superior to the others in the comparison.
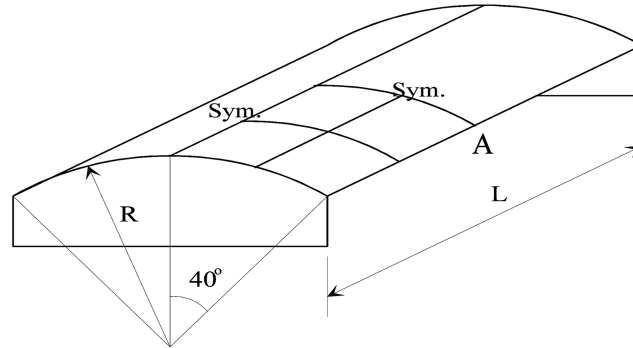
$$R = 25.0, L = 50.0, E = 4.32 \times 10^8, v = 0.0, h = 0.25, Uniform\,Load = 90$$

Fig. 14 Scodelis-Lo roof problem

Table 30 Results of Scordelis-Lo roof ($w_A = 0.3008$)

Element Size	Normalized Solutions				
	$\alpha\delta\beta$	$\alpha\delta\gamma$	$\beta\delta\gamma$	QUAD8*	QUAD8**
2 × 2	0.744	0.873	0.873	-	0.879
4 × 4	0.995	1.001	1.001	0.915 (5 × 5)	0.981
8 × 8	1.000	1.001	1.001	1.000 (9 × 9)	0.984 (6 × 6)

7. Conclusions

The main focus of this paper is to investigate on the performance of different patterns of sampling points for interpolating different components of shell strains. The 8-node ANS shell element using the sampling points earlier proposed (Bathe 1986, Lakshminarayana 1989, Bathe 1993, Kim 2003) is clearly a powerful element and has shown good convergence behavior in many problem solutions. However, previous works done in the area of ANS shell element neither showed the optimum combination of sampling points with an excellent accuracy nor removed the locking phenomenon.

It was found that the application of β pattern in transverse shear strain is the reason of the locking phenomenon in the analysis of straight beam using irregular mesh and thin plate. Thus, the limitation of application of the β pattern for the 8-node shell element is clearly revealed.

In order to improve the 8-node ANS shell element, based on a refined first-order shear deformation theory, a new combination of patterns of sampling points is adopted to analysis of plates and shells. The total strains are split into several components, and the suitable sampling point patterns are found for each component. A new combination of sampling point patterns ($\beta\delta\gamma$) for the in-plane normal, in-plane shear and transverse shear strain components can produce significantly better results while completely remove both membrane and shear locking even when full integration is used in the formulation. Optimality in the convergence behavior is retained and all strain components are predicted with reasonable accuracy.

The present combination of patterns of sampling points ($\beta\delta\gamma$) could be easily implemented into finite element code and used for the practical purpose. Future work will be useful to extend this work to dynamic analysis of isotropic and laminated composite shell structures.

Acknowledgements

References

Andelfinger, U. and Ramm, E. (1993), "EAS-elements for two dimensional, three-dimensional, plate and shell structures and their equivalence to HR-elements", *Int. J. Numer. Meth. Eng.*, **36**, 1311-1337.

Bathe, K.J. and Dvorkin, E.N. (1986), "A formulation of general shell elements-The use of mixed interpolation of tensorial components", *Int. J. Numer. Meth. Eng.*, **22**, 697-722.

Bathe, K.J., Lee, P.S. and Hiller, J.F. (2003), "Towards improving the MITC9 shell element", *Comput. Struct.*, **81**, 477-489.

Bucalem, M.L. and Bathe, K.J. (1993), "Higher-order MITC general shell elements", *Int. J. Numer. Meth. Eng.*, **36**, 3729-3754.

Choi, C.K., Lee, P.S. and Park, Y.M. (1999), "Defect-free 4-node flat shell element: NMS-4F element", *Struct. Eng. Mech.*, **8**, 207-231.

Han, S.C., Ham, H.D. and Kanok-Nukulchai, W. (2008), "Geometrically non-linear analysis of arbitrary elastic supported plates and shells using an element-based Lagrangian shell element", *Int. J. Nonlin. Mech.*, **43**, 53-64.

Han, S.C., Kim, K.D. and Kanok-Nukulchai, W. (2004), "An element-based 9-node resultant shell element for large deformation analysis of laminated composite plates and shells", *Struct. Eng. Mech.*, **18**, 807-829.

Han, S.C., Lee, S.Y. and Rus, G. (2006), "Postbuckling analysis of laminated composite plates subjected to the combination of the in-plane shear, compression and lateral loading", *Int. J. Solids Struct.*, **43**(18-19), 5713-5735.

Han, S.C., Tabiei, A. and Park, W.T. (2008), "Geometrically nonlinear analysis of laminated composite thin shells using a modified first-order shear deformable element-based Lagrangian shell element", *Compos. Struct.*, **82**, 465-474.

Hinton, E. and Huang, H.C. (1986), "A family of quadrilateral Mindlin plate elements with substitute shear strain fields", *Comput. Struct.*, **23**, 409-431.

Huang, H.C. (1989), *Static and Dynamic Analysis of Plates and Shells*. Springer-Verlag, London.

Kanok-Nukulchai, W. (1979), "A simple and efficient finite element for general shell analysis", *Int. J. Numer. Meth. Eng.*, **14**, 179-200.

Kim, K.D. and Park, T.H. (2002), "An 8-node assumed strain element with explicit integration for isotropic and laminated composite shells", *Struct. Eng. Mech.*, **13**, 1-18.

Kim, K.D., Lomboy, G.R. and Han, S.C. (2003), "A co-rotational 8-node assumed strain shell element for postbuckling analysis of laminated composite plates and shells", *Comput. Mech.*, **30**, 330-342.

Kim, K.D., Lomboy, G.R. and Voyiadjis, G.Z. (2003), "A 4-node assumed strain quasi-conforming shell element with 6 degrees of freedom", *Int. J. Numer. Meth. Eng.*, **58**, 2177-2200.

Lakshminarayana, H.V. and Kailash, K. (1989), "A shear deformable curved shell element of quadrilateral shape", *Comput. Struct.*, **33**, 987-1001.

Li, Z.X., Izzuddin, B.A. and Vu-Quoc, L. (2008), "A 9-node co-rotational quadrilateral shell element", *Comput. Mech.*, **42**, 873-884.

Ma, H. and Kanok-Nukulchai, W. (1989), "On the application of assumed strained methods", (Eds. Kanok-Nukulchai *et al.*), Structural engineering and construction, achievement, trends and challenges, AIT, Bankok.

MacNeal, R.H. and Harder, R.L. (1985), "A proposed standard set of problems to test finite element accuracy", *Finite Elem. Analy. Des.,* **1**, 3-20.

MacNeal, R.H. and Harder, R.L. (1992), "Eight nodes or nine?", *Int. J. Numer. Meth. Eng.,* **33**, 1049-1058.

Polit, O., Touratier, M. and Lory, P. (1994), "A new eight-node quadrilateral shear-bending plate finite element", *Int. J. Numer. Meth. Eng.,* **37**, 387-411.

Qi, Y., Knight, N.F. Jr. (1996), "A refined first-order shear-deformation theory and its justification by plane-strain bending problem of laminated plates", *Int. J. Solids Struct.,* **33**(1), 49-64.

Saleeb, A.F., Chang, T.Y. and Graf, W. (1987), "A quadrilateral shell element using a mixed formulation", *Comput. Struct.,* **26**, 787-803.

Simo, J.C., Fox, D.D. and Rifai, M.S. (1989), "A Stress Resultant Geometrically Exact Shell Model, Part II The Linear Theory; Computational Aspects", *Comput. Meth. Appl. Mech. Eng.,* **73**, 53-92.

STRAND 7, (2000), *Verification Manual,* G+D Computing Pty Ltd, Sydney.

Tanov, R. and Tabiei, A. (2000), "Simple correction to the first-order shear deformation shell finite element formulations", *Finite Elem. Analy. Des.,* **35**, 189-197.

Timoshenko, S.P. and Woinowosky-Krieger, S. (1959), *Theory of Plates and Shells,* McGraw-Hill, Kogakusa.

Wu, Z., Cheung, Y.K., Lo, S.H. and Chen W. (2008), "Effects of higher-order global–local shear deformations on bending, vibration and buckling of multilayered plates", *Compos. Struct.,* **82**(2), 277-289.

XFINAS, (2008), *Validation Manual,* available in www.xfinas.com.

Young, W.C. (1989), *Roark's Formulas for Stress and Strain.* 6th Edition, McGraw-Hill, New York.

Zienkiewicz, O.C. and Taylor, R.L. (1989), *The Finite Element Method,* McGraw-Hill, London.

Zienkiewicz, O.C. and Taylor, R.L. (2000), *The Finite Element Method,* Butterworth-Heinemann, London.